Numerical Modeling of Delayed Progressive Collapse of Reinforced Concrete Structures

Lívia Mello, S.M.ASCE[1]; Jia-Liang Le, M.ASCE[2]; and Roberto Ballarini, F.ASCE[3]

Abstract: There has been ever-increasing interest over the past decade in improving understanding of the mechanisms responsible for the progressive collapse of structures. Existing design recommendations and analyses are largely limited to instantaneous (time-independent) collapse. However, recent experiments revealed that reinforced concrete (RC) structures may be susceptible to delayed collapse, prompting the consideration of time-dependent material behavior as part of progressive collapse analysis and design. A reduced-order computational model for delayed collapse behavior of RC structures is introduced here in which the potential damage zones that evolve within a structure are treated as cohesive elements. The constitutive model of the cohesive element accounts for viscoelastic deformation and time-dependent damage accumulation of the concrete and hardening plasticity of the steel reinforcement. The remaining part of the structure is treated as a viscoelastic continuum. The model is first applied to simulate a pushdown experiment on a RC frame subassemblage under displacement-controlled loading. The deformation and failure mechanisms are in good agreement with experimental observations. The model is then used to investigate the behavior of the subassemblage in a "static fatigue scenario" in which the load is monotonically increased to a prescribed level and is then held constant until ultimate structural failure resulting from the assumed time-dependent response of the concrete material. The corresponding timescale of the delayed failure is on the order of hours, a result that has important implications not only for the analysis and design of RC structures against progressive collapse but also for the safety of first responders who enter structures that may collapse within that period of time. **DOI: 10.1061/(ASCE)EM.1943-7889.0001843.** © *2020 American Society of Civil Engineers.*

Introduction

Progressive collapse is a catastrophic large-scale structural failure caused by gravity-driven propagation of local structural damage. Research on progressive collapse dates back to the 1968 collapse of the Ronan Point apartment building. Since then, various prescriptive measures have been introduced into the code standards and design recommendations to mitigate the risk of such failures [GSA 2003; ASCE/SEI 7-10 (ASCE 2010); BSI 2006; DoD 2009; ICC 2009]. The likelihood of local structural damage caused by abnormal events such as explosion, blast, and object impact has seen a continuously increasing trend, as evidenced by tragic events such as the collapse of the Alfred P. Murrah Federal Building and the World Trade Center towers. As a consequence, there has been a continuously increasing interest in improving understanding of the underlying mechanisms involved in progressive collapse of structures and the development of performance-based design methodologies.

Progressive collapse may involve, among other things, material damage, crack propagation, large deformation, debris impact, and dynamic effects. Such complexity limits the capability of analytical modeling techniques (Bažant and Verdue 2007; Bažant et al. 2008; Pesce et al. 2012). In fact most existing analytical models are limited to simple cases where the motion of the collapse front can be considered as one-dimensional (1D). Direct experimental investigation of progressive collapse of structures offers important insights into the details of the failure mechanisms, but it is costly. Data is available only for a handful of full-scale collapse experiments on two- and three-dimensional (2D and 3D) structural frames subjected to local column removal (Lew et al. 2011; Sadek et al. 2011; Xiao et al. 2015). The limitations of analytical and experimental investigation have inspired major advances in numerical simulation of progressive collapse of buildings (Kunnath et al. 2018). Both continuum finite-element (FE) and discrete-element models have been used to simulate the progressive collapse behavior of reinforced concrete (RC) and steel buildings. The common drawback of these models is that the computational cost becomes prohibitive for large-scale buildings (Masoero et al. 2010; Alashker et al. 2011). To achieve a balance between model accuracy and computational efficiency, various reduced-order computational models, such as the damage-dependent beam element (Kaewkulchai and Williamson 2004; Grierson et al. 2005), macro-element-based modeling (Khandelwal and El-Tawil 2008; Bao et al. 2008), the applied element method (Helmy et al. 2012), and cohesive element modeling (Le and Xue 2014; Xue and Le 2016a, b), have been developed for RC buildings.

While the aforementioned modeling and experimental efforts have led to significant insights into the progressive collapse of RC structures and in turn to prescriptive code recommendations, they have focused on instantaneous collapse. In other words, currently available analysis tools assume that collapse occurs during the transient load redistribution caused by local structural damage. For instance, in some simplified analyses the structural resistance is checked against the dynamic load factor–enhanced gravity load (Sasani and Sagiroglu 2008). However, a recent experiment on a three-story, three-bay-by-three-bay RC frame (Xiao et al. 2015) showed delayed collapse for certain cases of column removal.

[1]Graduate Research Assistant, Dept. of Civil and Environmental Engineering, Univ. of Houston, Houston, TX 77204-4003.

[2]Associate Professor, Dept. of Civil, Environmental, and Geo-Engineering, Univ. of Minnesota, Minneapolis, MN 55455.

[3]Thomas and Laura Hsu Professor, Dept. of Civil and Environmental Engineering, Univ. of Houston, Houston, TX 77204-4003 (corresponding author). ORCID: https://orcid.org/0000-0002-4827-5818. Email: rballari@central.uh.edu

Note. This manuscript was submitted on March 20, 2020; approved on May 13, 2020; published online on July 23, 2020. Discussion period open until December 23, 2020; separate discussions must be submitted for individual papers. This paper is part of the ***Journal of Engineering Mechanics***, © ASCE, ISSN 0733-9399.

This observation drove home the point that the delayed collapse of RC structures is a new and potentially critical aspect of the assessment of structural vulnerability.

It has been speculated that time-dependent collapse of RC structures can be attributed to time-dependent material behaviors (Xiao et al. 2015). In fact, it is well known that concrete materials exhibit viscoelastic deformation under service loads, a phenomenon that has been extensively studied and for which numerous semiempirical models have been proposed [e.g., ACI 209.2R-08 (ACI 2008); Bažant and Murphy 1995; Gardner and Lockman 2001; Bažant and Jirásek 2018]. A large portion of these studies were motivated by rheological models, such as those of Kelvin and Maxwell. Some of these models have been implemented in FE analysis to simulate the long-term behavior of large-scale concrete bridges, including the Koror-Babeldaob Bridge in Palau (Bažant et al. 2012) and the I-35W St. Anthony Falls bridge in Minneapolis (Hedegaard et al. 2017).

Concrete materials exhibit viscoelastic deformation at relatively low levels of loading and time-dependent damage evolution at sufficiently higher levels. This damage phenomenon undoubtedly involves cracking and is therefore referred to as subcritical crack propagation or static fatigue. Early work by Rüsch showed that, under sustained loading, the strength of concrete significantly decreases with time (Rüsch 1960). Experiments also showed that static fatigue is strongly influenced by humidity (Krokosky 1973). Static fatigue of concrete can be modeled conveniently using fracture kinetics, as it has been for rocks and ceramics (Evans 1972; Thouless et al. 1983; Atkinson 1984; Evans and Fu 1984; Bažant and Le 2017). Note that the kinetics model has been used to investigate the effects of temperature and humidity on the fracture energy of concrete (Bažant and Prat 1988).

Though both time-dependent viscoelastic behavior and subcritical crack propagation have been studied for concrete materials, few studies have combined them into a single framework for the analysis of the time-dependent failure of RC structures. This study proposes a time-dependent computational model that incorporates both viscoelastic and subcritical damage accumulation mechanisms. The model is used for the numerical investigation of the delayed collapse behavior of RC structures.

Time-Dependent Reduced-Order Model of RC Structures

This study is anchored by a recently developed reduced-order computational model for time-independent progressive collapse of RC structures (Le and Xue 2014; Xue and Le 2016a, b), which adopts the concept of cohesive zone model that originated in the fracture mechanics community (Barenblatt 1959; Dugdale 1960; Bažant and Planas 1998). The inelastic behavior of a structure is characterized by a set of cohesive elements, which represent parts of the structure that could potentially be damaged. These parts, referred to as the potential damage zone (PDZ), are identified a priori based on the expected structural behavior (Le and Xue 2014; Xue and Le 2016a, b). For instance, in a column, the PDZs can be located at the midheight and two ends to simulate the Shanley column model (Bažant and Cedolin 1991). For beams, the PDZs can be placed at the ends and at the quarter span to capture catenary action and flexural failure. For more complex failure modes, such as diagonal shear failure in beams, more PDZs will be needed. The more PDZs are added, the model will converge to a nonlinear FE model. Note that the predefinition of PDZs in the present model is analogous to the predefinition of the crack path in the cohesive crack model. The parts of the structure that are not damaged are discretized using continuum elastic elements. Figs. 1(a and b) show

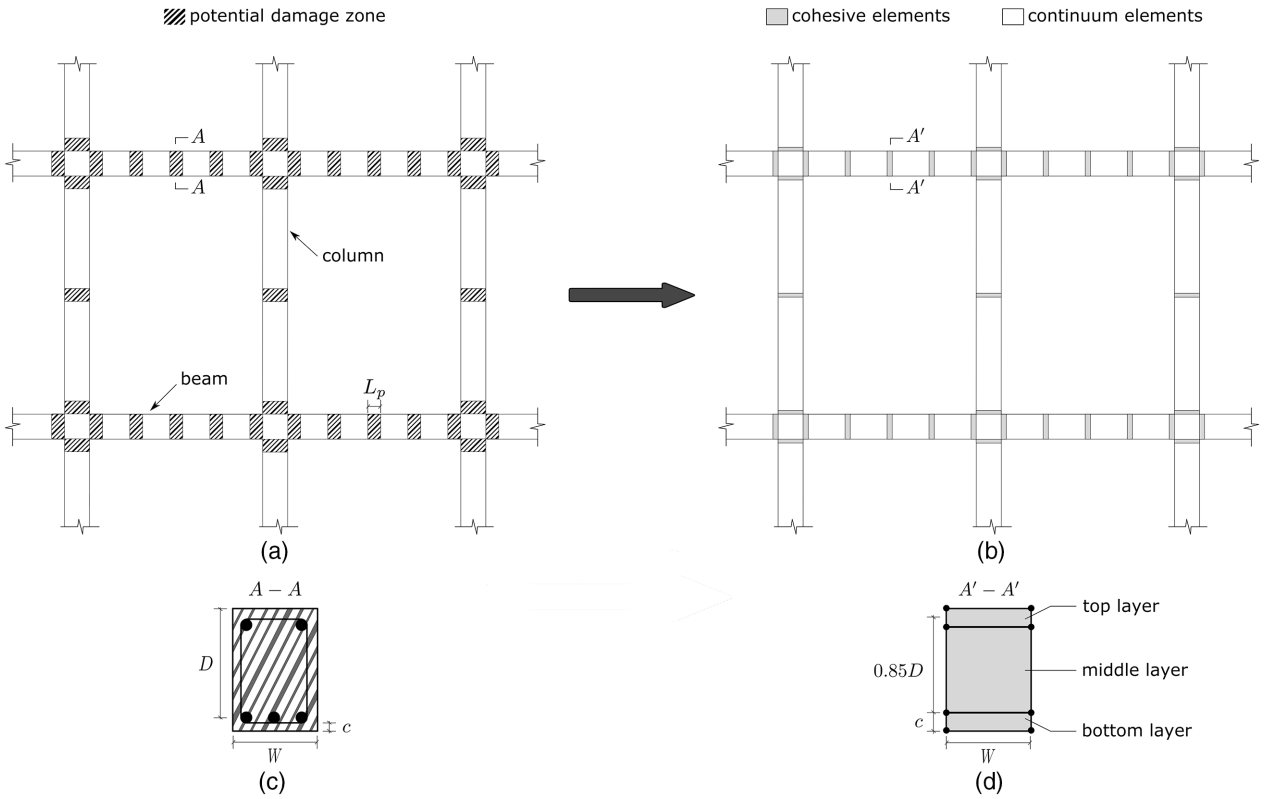

Fig. 1. Cohesive element based modeling of RC frame: (a) RC frame with PDZs; (b) numerical modeling of frame; (c) cross section of PDZ; and (d) cohesive element representation of PDZ.

J. Eng. Mech., 2020, 146(10): 04020113

the representation of a RC frame using a cohesive element model. In this study, this reduced-order model is extended to take into account the time-dependent behavior of concrete materials, including viscoelastic deformation and the aforementioned subcritical damage accumulation mechanism.

Following Le and Xue (2014) and Xue and Le (2016a, b), each PDZ consists of two components [Fig. 1(c)]: (1) effective concrete section, which is composed of concrete and shear reinforcement (if any), and (2) longitudinal reinforcement. The PDZ is represented by three cohesive elements; the top and bottom cohesive elements represent only the effective concrete section, and the middle element contains both the effective concrete section and longitudinal reinforcement [Fig. 1(d)]. The height c of the top and bottom cohesive elements corresponds to the thickness of the concrete cover, and the height of the middle element is chosen such that the distance from the midheight of the top element to the bottom surface of the middle element is equal to $0.85D$ [Fig. 1(d)], where D = effective depth of the section, which is equal to the distance between the centroid of the tensile reinforcement and the extreme material fiber in compression (Lowes and Altoontash 2003).

The total traction vector of a cohesive element can generally be written

$$\boldsymbol{\sigma}(w_n, w_m, w_l) = \boldsymbol{\sigma}^c(w_n, w_m, w_l) + \rho_s \boldsymbol{\sigma}^s(w_n, w_m, w_l) \tag{1}$$

where $\boldsymbol{\sigma} = (\sigma_n, \tau_m, \tau_l)^T$ = traction vector (σ_n, τ_m, τ_l = tractions in normal and two orthogonal shear directions); $\boldsymbol{\sigma}^c = (\sigma_n^c, \tau_m^c, \tau_k^c)^T$ = traction vector of effective concrete section; $\boldsymbol{\sigma}^s = (\sigma_n^s, \tau_m^s, \tau_k^s)^T$ = traction vector of longitudinal reinforcement; w_n = normal separation; w_l, w_m = shear separations; and ρ_s = longitudinal reinforcement ratio of cohesive element. In the following sections, the traction-separation relationship of each component is discussed.

Effective Concrete Section

To capture both the viscoelastic deformation and the subcritical damage accumulation mechanism of concrete, the effective concrete section is modeled by combining a fracturing unit and a chain of viscoelastic Kelvin units, as depicted in Fig. 2. The total tractions and displacements of the effective concrete section can be related to the tractions and displacements of the fracturing and viscoelastic chain elements as

$$\boldsymbol{\sigma}^c = \boldsymbol{\sigma}_f^c = \boldsymbol{\sigma}_{ve}^c \tag{2}$$

$$\boldsymbol{w} = \boldsymbol{w}_f + \boldsymbol{w}_{ve} \tag{3}$$

where $\boldsymbol{\sigma}^c$, $\boldsymbol{\sigma}_f^c$, and $\boldsymbol{\sigma}_{ve}^c$ = traction vectors of effective concrete section, fracturing unit, and viscoelastic chain, respectively; and $\boldsymbol{w}$, $\boldsymbol{w}_f$, and $\boldsymbol{w}_{ve}$ = displacement vectors of cohesive element, fracturing unit, and viscoelastic chain, respectively.

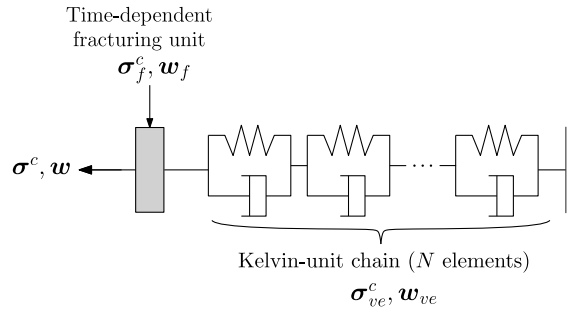

Fig. 2. Constitutive model of effective concrete section.

Fracturing Unit

As shown in Fig. 2, the damage and failure of the effective concrete section is governed by the fracturing unit. The constitutive model of the fracturing unit is introduced by defining the effective displacement as $\bar{w}_f = \sqrt{w_{fn}^2 + \alpha_i(w_{fm}^2 + w_{fl}^2)}$, where w_{fn}, w_{fm}, and w_{fl} are the normal and two orthogonal shear displacements of the fracturing unit, respectively, and $\alpha_i (i = t, c)$ are constants corresponding to tension-shear loading and compression-shear loading, respectively. The mode mixity angle is defined as $\theta = \tan^{-1}\left(w_{fn}/\alpha_i\sqrt{w_{fm}^2 + w_{fl}^2}\right)$. The work-conjugate effective traction $\bar{\sigma}^c$ satisfies $\bar{\sigma}^c \delta\bar{w}_f = \sigma_{fn}^c \delta w_{fn} + \tau_{fm}^c \delta w_{fm} + \tau_{fl}^c \delta w_{fl}$, which implies $\sigma_{fn}^c = \bar{\sigma}^c \sin\theta$, $\tau_{fm}^c = \alpha_i \bar{\sigma}^c \cos\theta \sin\psi$, and $\tau_{fl}^c = \alpha_i \bar{\sigma}^c \cos\theta \cos\psi$, where $\psi = \tan^{-1}(w_{fm}/w_{fl})$. Therefore, the constitutive response of the fracturing unit can be fully described by the relationship between $\bar{\sigma}^c$ and $\bar{w}_f$.

Here a damage-mechanics based constitutive law is proposed for the $\bar{\sigma}^c - \bar{w}_f$ relationship, i.e.

$$\bar{\sigma}^c = (1 - d)E\bar{w}_f \tag{4}$$

where d = damage parameter ranging from 0 (virgin state) to 1 (fully damaged state); and E = elastic stiffness. By assuming that the cohesive element exhibits a linear elastic behavior up to the peak strength, the elastic stiffness can be expressed as $E = \sigma_p/w_y$, where σ_p is the peak strength of the fracturing unit and w_y the corresponding displacement at σ_p. For mixed-mode loading, it is expected that σ_p and w_y vary with the mode mixity. Following Le and Xue (2014) and Xue and Le (2016a, b), it is assumed that

$$\sigma_p = |\sigma_{ip}|(\sin|\theta|)^{\beta_i} + \alpha_i^{-1}|\sigma_{\tau p}|(\cos|\theta|)^{\beta_i} \tag{5}$$

$$w_y = [(|w_{iy}|\sin|\theta|)^{\gamma_i} + (|w_{\tau y}|\cos|\theta|)^{\gamma_i}]^{1/\gamma_i} \tag{6}$$

where $\sigma_{ip} (i = t, c)$ = maximum tensile and compressive strengths of the effective concrete section, respectively; $\sigma_{\tau p}$ = shear strength of the effective concrete section; $w_{iy} (i = t, c)$ = separations at which cohesive traction reaches σ_{ip} under pure tensile and compressive loading, respectively; $w_{\tau y}$ = separations at which cohesive traction reaches $\sigma_{\tau p}$ under pure shear loading; and β_i, $\gamma_i (i = t, c)$ = calibrated constants that describe tension-shear interaction and compression-shear interaction, respectively.

The rate-dependent fracture behavior that evolves the damage is treated using a growth kinetics model. A widely used fracture kinetics model for quasi-brittle materials under sustained load is the Evans law (Evans 1972; Thouless et al. 1983; Evans and Fu 1984; Bažant et al. 2009; Bažant and Le 2017), in which the crack growth rate is expressed as a power-law function of the stress intensity factor. Another commonly used model for subcritical damage growth is based on continuum damage mechanics (Kachanov 1986, 1994; Lemaitre and Desmorat 2005; Rabotnov 1969), in which the damage growth rate is related to the effective traction:

$$\frac{\mathrm{d}d}{\mathrm{d}t} = \frac{B\lambda^k}{(1 - d)^r} \tag{7}$$

where B, k, r = constants; and $\lambda = \bar{\sigma}^c/\sigma_p$ = relative load level. For any given loading history, the combination of Eqs. (7) and (4) dictates the loading path in the traction-separation space. To recover the behavior under quasi-static monotonic loading conditions,

the loading path is bounded by a bilinear traction-separation envelope, which is expressed by

$$\bar{\sigma}^c(\bar{w}_f) = \begin{cases} \sigma_p \bar{w}_f / w_y & (\bar{w}_f \le w_y) \\ \sigma_p (w_u - \bar{w}_f)/(w_u - w_y) & (w_y < \bar{w}_f \le w_u) \\ 0 & (w_u < \bar{w}_f) \end{cases} \quad (8)$$

where $w_u = [(|w_{iu}| \sin|\theta|)^{\gamma_i} + (|w_{\tau u}| \cos|\theta|)^{\gamma_i}]^{1/\gamma_i}$; $w_{iu}(i = t, c)$ = separations at which the normal traction vanishes under pure tensile and compressive loading, respectively; and $w_{\tau u}$ = separation at which shear traction vanishes under pure shear loading. It can be shown that, under a sufficiently fast, quasi-static, and monotonically increasing displacement-controlled load, the traction-separation response calculated by Eqs. (4) and (7) would follow Eq. (8).

Viscoelastic Unit

For delayed progressive collapse, the time scale of interest is on the order of hours to a few days. Therefore, the long-term creep behavior need not be considered. The viscoelastic strain can be expressed by Bažant and Prasannan (1989):

$$\boldsymbol{w}_{ve}(t) = \epsilon_{ve}(t) L_p = \left\{ \int_0^t \Phi(t - t_0) \boldsymbol{G} \dot{\boldsymbol{\sigma}}^c(\tau) d\tau \right\} L_p \quad (9)$$

where L_p = length of PDZ [Fig. 1(a)]; $\epsilon_{ve}(t)$ = strain in viscoelastic unit at time t; $\Phi(t - t_0)$ = nonaging compliance function of concrete; $t - t_0$ = loading time (t_0 = time of start of loading); and matrix $\boldsymbol{G}$ accounts for the normal-shear coupling behavior of the effective concrete section (Alnaggar et al. 2017):

$$\boldsymbol{G} = \begin{bmatrix} 1 & 0 & 0 \\ 0 & 1/\alpha_i^2 & 0 \\ 0 & 0 & 1/\alpha_i^2 \end{bmatrix} \quad (10)$$

The viscoelastic response of concrete is modeled using a nonaging Kelvin chain (Fig. 2), and therefore the compliance function $\Phi(t - t_0)$ can be approximated by the Dirichlet series (also called as Prony Series) (Bažant and Jirásek 2018)

$$\Phi(t - t_0) \approx A_0 + \sum_{j=1}^{N} A_j \left[1 - \exp\left(-\frac{t - t_0}{\tau_j} \right) \right] \quad (11)$$

where A_0 = elastic compliance that accounts for instantaneous deformation; and A_j and τ_j = corresponding compliance and relaxation time of jth Kelvin unit ($j = 1, \ldots, N$), respectively. Previous studies suggested choosing τ_j in base-10 geometric progression [i.e., $\Delta(\log \tau_\mu) = 1$] to obtain a sufficiently smooth compliance curve (Bažant and Xi 1995; Bažant and Jirásek 2018). The elastic compliance A_j can then be determined based on the continuous retardation spectrum (Bažant and Xi 1995).

Longitudinal Reinforcement

The constitutive behavior of the longitudinal reinforcement is formulated based on the uniaxial stress-strain relation of steel material modified by the bond-slip effect, i.e.

$$\epsilon^s(\sigma^s) = \epsilon_0^s(\sigma^s) + \frac{\Delta_s(\sigma^s)}{L_p} \quad (12)$$

where σ^s = actual bar stress; $\epsilon_0^s(\sigma^s)$ = bar strain without considering bond-slip effect; and Δ_s = total slip at bar stress σ_n^s. The total slip $\Delta_s(\sigma_n^s)$ can be determined based on an assumed stress distribution along the concrete–reinforcement interface (Sezen and Moehle 2003; Lew et al. 2011). The ultimate bar strength is governed by the minimum of the steel rupture strength and the bar pullout strength. The bar pullout strength can be calculated from the concrete and steel properties based on the ACI recommendation [ACI 408R-03 (ACI 2003)]. Eq. (12) can be rewritten as $\sigma^s = f(\epsilon^s)$.

Note that the contribution of the longitudinal reinforcement to the load resistance of the cohesive element depends on the loading scenario. Under tension, the load-carrying capacity of longitudinal reinforcement can be fully achieved even after the concrete material is damaged. While under compression the reinforcement would buckle and lose load-carrying capacity as soon as the concrete is fully damaged.

The traction-separation relation of the longitudinal reinforcement can be easily obtained by projecting the aforementioned uniaxial stress-strain relation onto the normal and shear directions. The total bar elongation within the PDZ is approximated as $w = \sqrt{(L_p + w_n)^2 + w_m^2 + w_l^2} - L_p$, and the angle between the direction of the bar stress and the normal direction by $\phi = \tan^{-1}\left[\sqrt{w_m^2 + w_l^2}/(L_p + w_n)\right]$. Consequently, the normal and shear tractions in the bar are given by $\sigma_n^s = f(w/L_p)\cos\phi$, $\tau_m^s = f(w/L_p)\sin\phi\sin\psi$, and $\tau_l^s = f(w/L_p)\sin\phi\cos\psi$. The angle ϕ is usually small, and therefore the longitudinal reinforcement has a minimal effect on the shear behavior of the PDZ. The unloading and reloading paths for the longitudinal reinforcement are described by the classical linear isotropic kinematic hardening model (Xue and Le 2016b). Note that during the progressive collapse, the strain rate is relatively low, and therefore a rate-independent constitutive model for steel reinforcement is sufficient for the present analysis.

It is worth noting that the bond slip, a type of interfacial fracture, could also exhibit a time-dependent behavior. The time dependence may be described by some fracture kinetics model, such as the Evans law. However, there is a lack of experimental data on the bond-slip behavior under static fatigue. The potential time dependence of bond slip is worth further investigation as it could have a considerable influence on the delayed collapse behavior of the overall structure.

Elements Outside Potential Damage Zones

The structure outside the PDZs is modeled by standard continuum elements. Based on the present model, these elements do not contribute to the overall structural failure. Nevertheless, they share the same viscoelastic behavior as the PDZs, so that no discontinuity will arise during the time-dependent elastic response. This assumption ensures a smooth elastic stress distribution throughout the structure.

Numerical Implementation

The time-dependent cohesive model is implemented as a user-defined material subroutine in the commercially available software ABAQUS for explicit FE analysis. During the ith time increment $\Delta t_i = t(i + 1) - t(i)$, the increment of cohesive separation $\Delta \boldsymbol{w}^{(i)}$ is prescribed. The corresponding traction increment $\Delta \boldsymbol{\sigma}^{s,i}$ of the longitudinal reinforcement can directly be calculated based on the modified stress-strain relation [Eq. (12)].

For the effective concrete section, Eqs. (2) and (3) require $\Delta \boldsymbol{w}^i = \Delta \boldsymbol{w}_f^{c,i} + \Delta \boldsymbol{w}_{ve}^{c,i}$ and $\Delta \boldsymbol{\sigma}^{c,i} = \Delta \boldsymbol{\sigma}_f^{c,i} = \Delta \boldsymbol{\sigma}_{ve}^{c,i}$. For the viscoelastic unit, the stress calculated from the previous time step is used to determine the strain increment of each Kelvin unit. This leads to

J. Eng. Mech., 2020, 146(10): 04020113

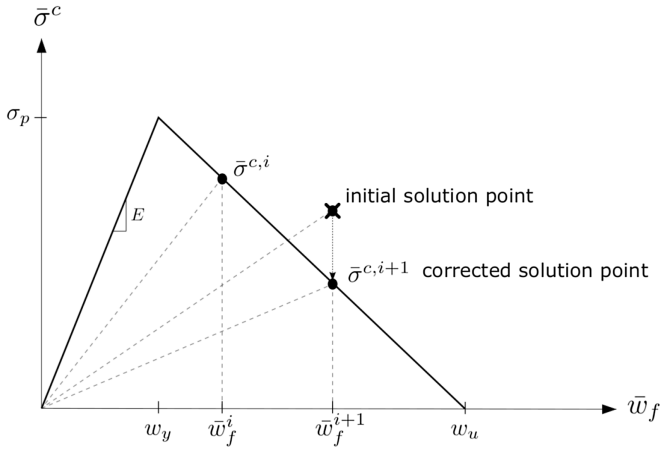

Fig. 3. Numerical correction scheme for solution point that is outside traction-separation envelope.

$$\Delta\boldsymbol{\epsilon}_{ve,j}^{c,i} = [\boldsymbol{G}A_j\boldsymbol{\sigma}^{c,i} - \boldsymbol{\epsilon}_{ve,j}^{c,i}][1 - \exp(-\Delta t_i/\tau_j)] \tag{13}$$

where $\boldsymbol{\sigma}^{c,i}$, $\boldsymbol{\epsilon}_{ve,j}^{c,i}$ = traction vector and strain vector of each Kelvin unit calculated from the previous time step, respectively. The total increment in the separation of the viscoelastic unit is simply given by $\Delta\boldsymbol{w}_{ve}^{c,i} = L_p \sum_{j=0}^{N} \Delta\boldsymbol{\epsilon}_{ve,j}^{c,i}$.

By subtracting $\Delta\boldsymbol{w}_{ve}^{c,i}$ from $\Delta\boldsymbol{w}^i$, the separation increment $\Delta\boldsymbol{w}_f^i$ of the fracturing unit is obtained. Noting that the present constitutive model of the fracturing unit can be rewritten as $\boldsymbol{\sigma}_f^{c,i} = (1-d)\boldsymbol{C}(\boldsymbol{w}_f)\boldsymbol{w}_f$, where $\boldsymbol{C}$ = a second-order stiffness tensor, which depends on the mode mixity. This constitutive equation can be expressed in incremental form, i.e.

$$\Delta\boldsymbol{\sigma}_f^{c,i} = -\boldsymbol{C}^i\boldsymbol{w}_f\Delta d^i + (1-d^i)\left(\boldsymbol{C}^i + \boldsymbol{w}_f^i\frac{\mathrm{d}\boldsymbol{C}}{\mathrm{d}\boldsymbol{w}_f}\bigg|_{\boldsymbol{w}_f^i}\right)\Delta\boldsymbol{w}_f^i \tag{14}$$

where Δd^i = increment of damage variable during present time increment; and all other quantities with subscript i carry the values calculated from the previous time step. The damage variable increment is calculated from the damage accumulation model [Eq. (7)], i.e., $\Delta d^i = B(1-d^i)^{-r}(\bar{\sigma}_c^i/\sigma_p^i)^k\Delta t_i$. Once the traction increment is calculated, it is checked whether the total traction falls outside the bilinear traction-separation envelope described by Eq. (8). If it does, the traction is corrected by bring it back onto the envelope (Fig. 3).

As mentioned earlier, elements inside and outside the PDZs must exhibit the same viscoelastic behavior. For the sake of convenience, the continuum elements outside the PDZs are modeled using a built-in viscoelastic material model in ABAQUS. The time-dependent properties are input through a normalized bulk compliance function. This function is numerically calibrated so that it yields the same compliance as predicted by the Dirichlet series approximation for the viscoelastic unit of the PDZ [Eq. (11)].

Simulation of RC Structural Subassemblage

Description of Numerical Study

The model is applied to the analysis of the collapse behavior of a RC frame subassemblage. A commonly used experiment for investigating structural collapse behavior is the pushdown test, in which a downward displacement control loading is applied all the way to failure. Owing to the large deformation involved in the response, the failure process consists of various mechanisms, such as concrete fracture and damage, reinforcement yielding and rupture, catenary and membrane actions, all of which are relevant.

Consider the full-scale pushdown test performed by NIST (Lew et al. 2011), as shown in Fig. 4(a). In the experiment, the middle column head was pushed downward in a quasi-static manner until the structure failed. Fig. 4(b) shows the measured load-displacement curve, which consists of an initial softening branch followed by a significant hardening regime. The initial softening behavior can be attributed to concrete compressive damage that occurs at the interior joints of the beams. Under the continuing displacement, catenary action develops in the beams and is active up to the rupture of the longitudinal reinforcement.

Not only is the NIST experiment modeled here, but also is the delayed collapse produced by a representative different loading protocol: the applied displacement is increased monotonically until the load reaches a level P that is lower than the first peak load P_c measured in the pushdown experiment, and then the load is held constant all the way until failure. The failure mechanism is largely governed by the time-dependent damage accumulation and load redistribution. The key output of the simulation is the time to failure t_f (structural lifetime). The aforementioned loading scenario represents the case in which the structure survives after experiencing local structural damage (such as column removal) and subsequently sustains increased gravity loads. Since the interest of this study is delayed collapse behavior, in which the timescale is on the order of a few days at maximum, the simulation involves only high load levels, i.e., $P/P_c = 0.98, 0.97, 0.96, 0.95, 0.94$, and 0.93. These simulations provide the load-lifetime curve of the frame.

Determination of Model Parameters

In the present reduced-order model, the model parameters of the cohesive element represent the behavior of a PDZ. The cohesive model has three main components: (1) fracturing unit of the effective concrete section, (2) viscoelastic unit of the effective concrete section, and (3) longitudinal reinforcement. As discussed in the section "Longitudinal Reinforcement," the cohesive parameters of the longitudinal reinforcement can be obtained directly based on the stress-strain curve of steel material and an analytical model of bond slip. The calibration of the model parameters of the effective concrete section is more involved. Previous studies suggested that these parameters could be determined by a set of fine-scale FE simulations (Le and Xue 2014; Xue and Le 2016a, b), which involves a sophisticated constitutive model for concrete. In a recent study (Le and Xue 2014), a time-independent cohesive model was used to simulate the NIST pushdown test, where the behavior of the effective concrete section was described by a bilinear traction-separation law with the same form as Eq. (8). Therefore, the result of this previous study is used to construct the traction-separation envelope of the fracturing unit of the present model. What remains to be calibrated are the viscoelastic model and the damage accumulation model.

The viscoelastic behavior of concrete has been extensively studied. It suffices to consider the following function for nonaging compliance of concrete (Bažant and Xi 1995):

$$\Phi(t-t_0) = \xi_1 \ln[1 + (t-t_0)^n] \tag{15}$$

where $n = 0.1$. This compliance function can be approximated by a chain of 10 Kelvin units with retardation times ranging from 10^{-4} to 10^5 days (Alnaggar et al. 2017). By matching Eq. (11) with Eq. (15), the elastic compliance $A_0 = 0.642\xi_1$ is obtained, and

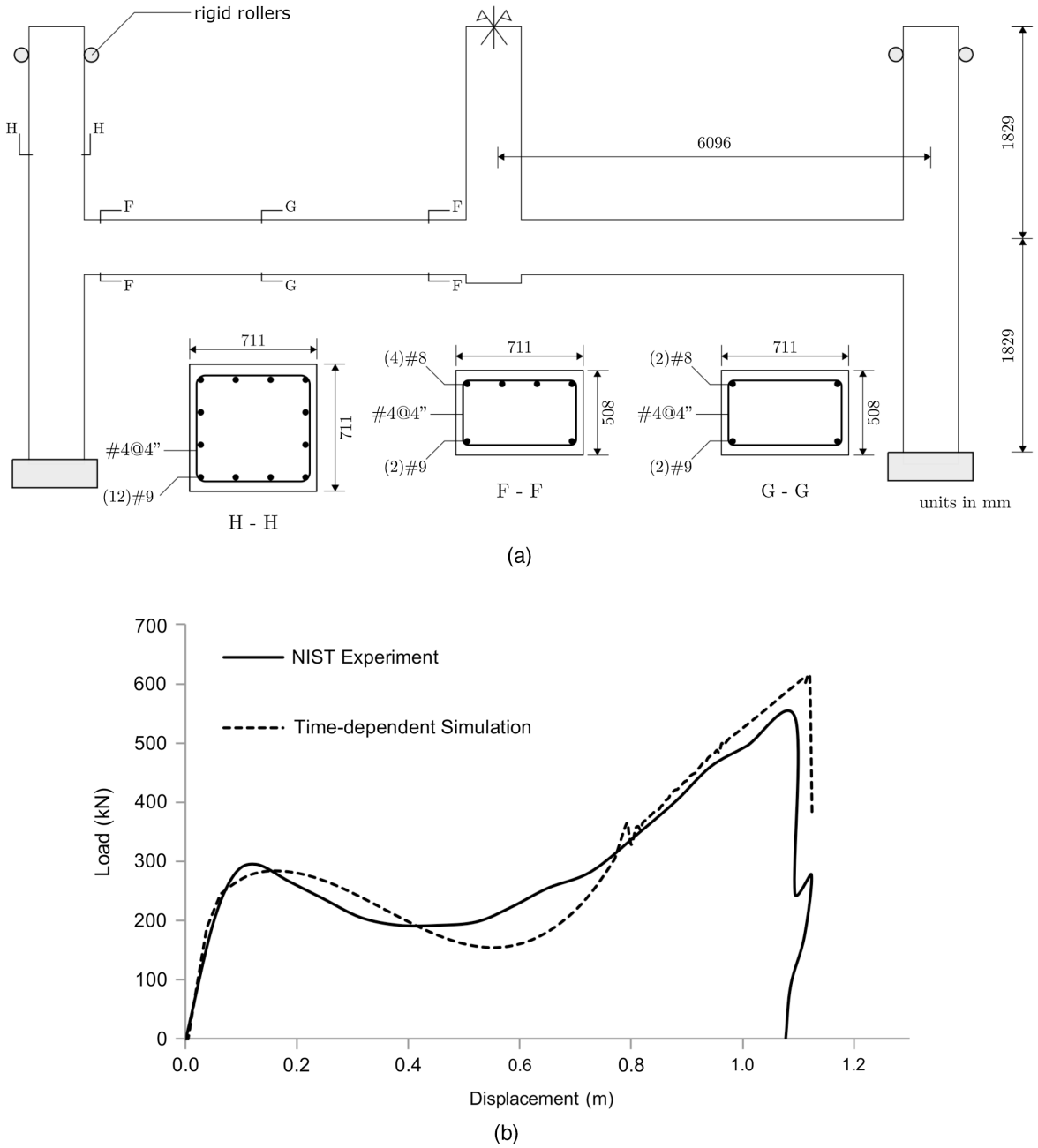

Fig. 4. NIST pushdown experiment: (a) geometry and dimension of test specimen; and (b) comparison between measured and simulated load-deflection curves.

ξ_1 can be related empirically to the concrete properties (Bažant and Murphy 1995). Other compliances A_j can be calculated as $A_j = L_j \Delta(\log \tau_j) \ln 10 \approx L_j \ln 10$, where the fact that the retardation times are chosen in a base-10 geometric progression is used. L_j can be estimated from the continuous retardation spectrum of order 3 of function $\Phi(t - t_0)$ (Bažant and Xi 1995; Alnaggar et al. 2017), i.e.

$$L_j = \frac{\xi_1 (3\tau_j)^3}{2} \left\{ \frac{n(n-2)(3\tau_j)^{n-3}[n-1-(3\tau_j)^n] - n^2(3\tau_j)^{2n-3}}{[1+(3\tau_j)^n]^2} - \frac{2n^2(3\tau_j)^{2n-3}[n-1-(3\tau_j)^n]}{[1+(3\tau_j)^n]^3} \right\} \tag{16}$$

The damage accumulation model [Eq. (7)] is an essential component of the model. However, determination of the damage accumulation parameters for concrete materials is not a trivial task. There are very limited experimental data available on the damage behavior of concrete under sustained loading (Rüsch 1960; Bažant and Prat 1988; Zhou 1992). Time-dependent damage accumulation in concrete is affected by a number of factors, such as the material composition and external environment (e.g., humidity). No information is available on the damage accumulation behavior of concrete that was used in the NIST test. Therefore, in this study, the parameters B, k, r of Eq. (7) are chosen so that the effective concrete section exhibits a reasonable load-lifetime curve under sustained compressive loading. Compressive loading is chosen because in the present static fatigue simulation, the time-dependent failure of the frame subassemblage is governed by the compressive failure of concrete. The tension resistance of the beam is contributed by the longitudinal reinforcement.

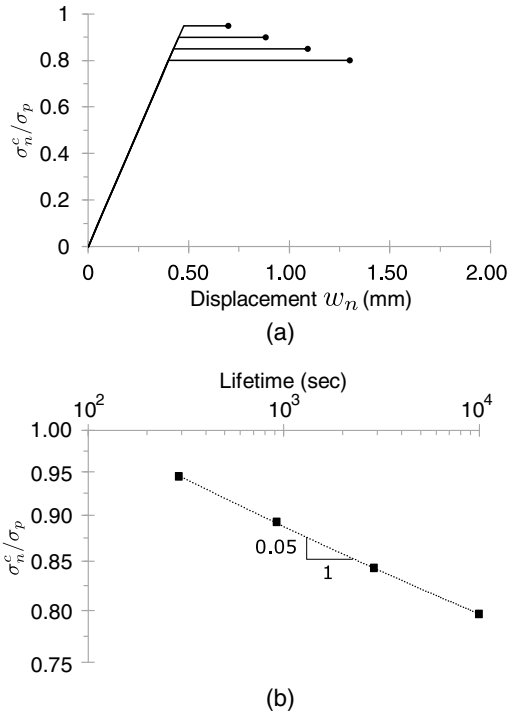

Fig. 5. Static fatigue response of cohesive element effective concrete section under compression: (a) load-displacement history; and (b) load-lifetime curve.

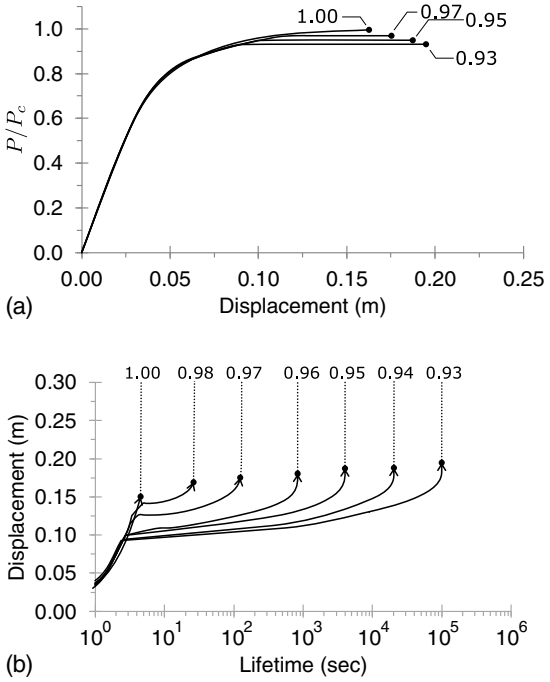

Fig. 6. Simulated delayed failure behavior of frame subassemblage: (a) load-displacement history; and (b) time evolution of displacement at center column head.

To simulate the load-lifetime curve of the cohesive element effective concrete section, first the load is monotonically increased at a sufficiently fast rate to a prescribed level before the peak, and then held constant until failure. Note that in the simulation the element suffers no damage at the end of the monotonic loading stage (i.e., no stiffness degradation) [Fig. 5(a)]. After several trials, $B = 1.5 \times 10^{-3}/s$, $k = 20$, and $r = 5$ are chosen, which yields the load-lifetime curve as shown in Fig. 5(b). It is seen that the load-lifetime relationship exhibits an inverse power-law dependence, which is a consequence of the power-law form of the damage accumulation model [Eq. (7)]. The power exponent of the load-lifetime curve is approximately $-1/20$, a value that is similar to the load-lifetime exponent measured in Rüsch's experiments (Rüsch 1960). Meanwhile, it is noted that the present damage accumulation model [Eq. (7)] is analogous to the Evans law for subcritical crack growth, and its stress dependence (i.e., $\mathrm{d}d/\mathrm{d}t \propto \sigma^{20}$) is also consistent with $\mathrm{d}a/\mathrm{d}t \propto \sigma^k$ (a = crack length, $k \sim 10 - 30$) in the Evans law (Bažant et al. 2009).

Results and Discussion

NIST Pushdown Test

The proposed model is first used to simulate the NIST pushdown test. In the simulation, a linearly ramped displacement is applied at the middle column head at a rate of 25 mm/min (Lew et al. 2011), until ultimate failure. As shown in Fig. 4(b), the simulated load-displacement curve matches the experimental measurement reasonably well. In the simulation, the frame first exhibits a linear elastic response, and the opposite positions of the compression zone of the beam at the middle and exterior columns cause an arch effect. Upon continued loading, the top cohesive elements at the interior joints of the beam start to experience compressive damage, which causes a shifting of the neutral axis and a decrease in the load-carrying capacity. A further increase in displacement eventually leads to the development of catenary action, where the entire beam is in tension. The ultimate failure of the frame is associated with rupture of the longitudinal reinforcement. These simulated mechanisms agree well with the experimental observation reported in Lew et al. (2011).

Simulation of Delayed Failure

The model is now used to simulate delayed failure behavior. Fig. 6(a) presents the simulated load-displacement curves. It is seen that all loading cases associated with the delayed failure simulations share the same ascending branch. Under different levels of sustained loading, the frame assemblage fails at different displacements. As expected, the ultimate displacement increases mildly with a decreasing sustained load. On the other hand, the sustained load has a significant effect on the time to failure. Fig. 6(b) shows the time evolution of the displacement at the middle column head. It is observed that the displacement increases slowly under sustained loading, and at the ultimate failure point, the displacement suddenly starts to grow at a very fast rate.

The aforementioned delayed failure behavior is attributed to the time-dependent damage accumulation mechanism. Eq. (7) indicates a continuous material damage growth under constant loads. The damage growth deteriorates the overall load-carrying capacity of the structure. As the load-carrying capacity drops below the sustained load prescribed in the analysis, the damage propagates dynamically in an unstable manner, signified by a sudden increase in displacement. Based on the failure mechanism of the NIST experiment, it is expected that the time-dependent failure observed in the present delayed failure simulation will be dominated primarily by the compressive damage of concrete at the interior joints of the beam. Fig. 7 presents the time evolution of the compressive damage at the interior joints. It is seen that the damage growth history consists of three stages: (1) fast damage growth due to monotonically

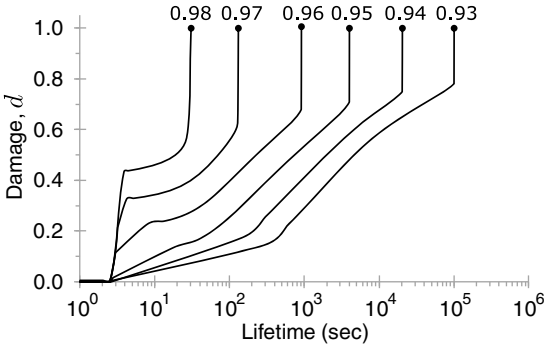

Fig. 7. Time history of damage growth in top cohesive element of interior beam joint.

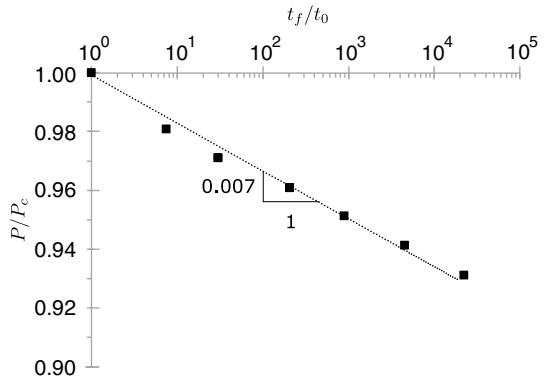

Fig. 8. Simulated load-lifetime curve of frame subassemblage.

increasing load, (2) slow subcritical damage growth under sustained load, and (3) dynamic and unstable damage growth.

It is observed that the first stage of the damage growth is significantly influenced by the applied load level. As the applied load approaches the peak load capacity of the frame, compressive damage occurs in the top cohesive element of the interior beam joint, and this initial damage level is very sensitive to the applied load in the prepeak regime. The effect of the applied load on the second stage of the damage growth can be attributed to the initial damage level caused by the first monotonic loading. Based on Eq. (7), a low initial damage level will lead to very slow damage growth and, therefore, a much longer lifetime. In such a case, the viscoelastic behavior of concrete will have a considerable influence on the load redistribution mechanism and overall collapse behavior. Note also that Fig. 7 corresponds exactly to the time history of the displacement [Fig. 6(b)], and this correspondence clearly indicates the governing role of time-dependent accumulation of compressive damage in the overall delayed collapse behavior.

Fig. 8 plots the simulated load-lifetime curve of the frame subassemblage in logarithmic scales. The load-lifetime relation can be well fitted by an inverse power law, i.e.

$$P/P_c = (t_f/t_0)^{-0.007} \tag{17}$$

where t_0 = time to reach first peak load in the simulation of $P/P_c = 1$.

Note that the inverse power-law form of the load-lifetime curve [Eq. (17)] is consistent with what has been reported in a number of experimental and numerical studies on the creep-rupture behavior of concrete specimens (Carpinteri et al. 1997; Luzio 2009; Boumakisa et al. 2018). On the other hand, it is worthwhile to point out that the magnitude of the power-law exponent of the load-lifetime curve of the frame subassemblage is much smaller than that of the cohesive element itself [Fig. 5(b)], even though the overall delayed collapse behavior is governed by the damage growth of the cohesive element. In other words, the frame subassemblage exhibits a much more pronounced load effect on the structural lifetime.

To understand this difference, it is noted that, even though the subassemblage is subjected to a constant load, the loading on the individual cohesive elements varies with time. Fig. 9 shows the time histories of individual forces in the cross section of the interior joint of the beam for different load levels. From the top row of Fig. 9 it is seen that the net force on the cross section turns to compression as the displacement increases. This is because the increasing displacement causes the beams to be pushed outward. Meanwhile, the beam motion is restrained by the side columns, thereby generating a net compressive force in the beam.

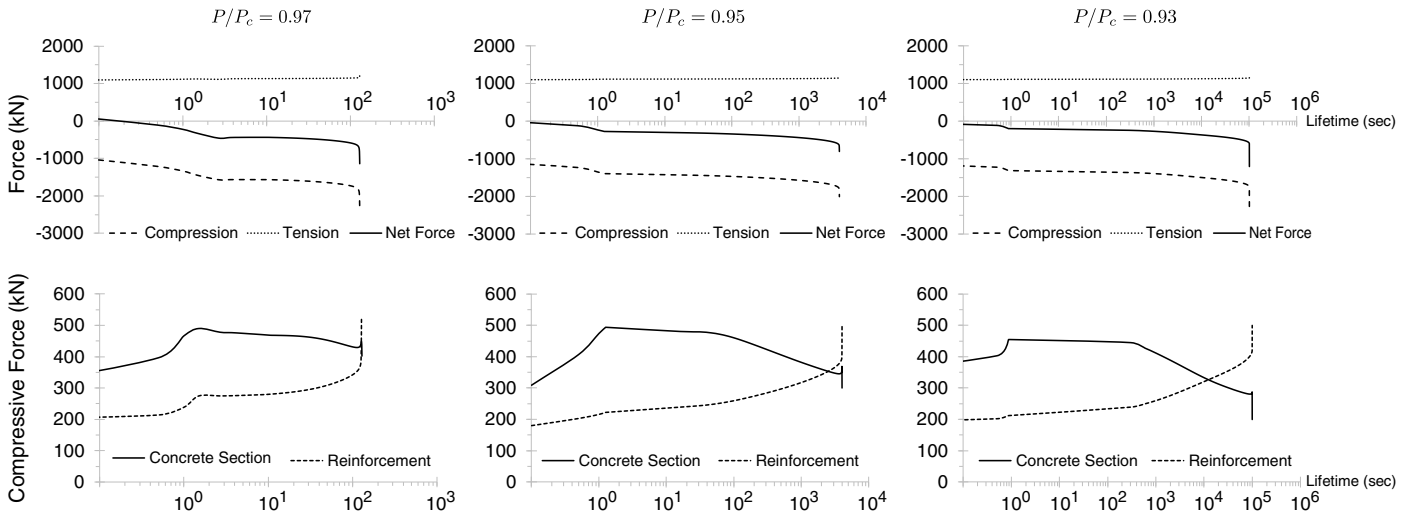

Fig. 9. Time histories of individual forces in cross section of interior joint of beam under different load levels.

The bottom row of Fig. 9 shows the individual compressive forces in the concrete section and steel reinforcement. It is found that the compressive force in the reinforcement continuously increases with time, whereas the concrete section experiences a decrease in compressive force over the major part of the loading duration. This is because in the model, the concrete section and the reinforcement share the same displacement. Owing to the time-dependent damage accumulation and viscoelastic deformation of concrete, the elongation of reinforcement is increasing over time, indicating a larger compressive stress. However, the overall loading on the structure is prescribed, and therefore the compressive stress in the concrete section must decrease. This decrease directly results in a significant reduction in the damage growth rate and, consequently, a significantly longer structural lifetime. Fig. 9 shows that the decrease in compressive force in the concrete section becomes more significant for lower load levels owing to the larger deformation experienced by the top cohesive element.

The foregoing analysis indicates the potential influence of time-dependent bond-slip behavior on the delayed collapse behavior. The time dependence of bond slip will certainly affect the distribution of compressive forces in the concrete section and reinforcement. It is expected that the time-dependent increase in bond slip under constant loads will make the reinforcement behave more independently from the concrete section, which implies an increasing compression in the concrete section. This increase will lead to a much higher rate of damage growth in concrete and, therefore, accelerate structural collapse.

When the applied load level is sufficiently high ($P/P_c > 95\%$), the reduction in compression in the concrete section is insignificant. However, note that the cohesive element experiences a considerable level of compressive damage at the end of the monotonic loading stage (Fig. 7). This is very different from the simulation of the load-lifetime curve of a single cohesive element [Fig. 5(a)], in which the monotonic loading stage does not introduce any damage to the element. Based on Eq. (7), the predamage level strongly affects the damage growth rate, as well as the total damage increment before ultimate failure is reached. This mechanism contributes significantly to the strong load effect on the structural lifetime of the frame subassemblage subjected to a high level of sustained loading.

Implications for Analysis of Progressive Collapse

The present simulation results indicate that the time-dependent behavior of concrete could lead to a delayed failure response of RC structures. This finding has important implications for the analysis of progressive collapse. The structural resistance against progressive collapse is often assessed by the alternative load path analysis (DoD 2009), which considers the sudden loss of some critical load-bearing structural members (usually columns or walls). It is expected that after the sudden removal of a column or a wall, the transient loading could cause significant damage to adjacent structural members. On the other hand, the damage may not be severe enough to cause incipient collapse. Once the redistribution of the gravity load stabilizes, the gravity loading on these adjacent structural members would be significantly higher than previously. In the existing alternative load path analysis, as long as the capacity of the structural members exceeds the transient gravity loading, the structure is considered to be safe for the particular column/wall removal scenario.

The results of the present study raise another new and important consideration. Though structural members may not fail immediately after the sudden removal of a column/wall, they could suffer some level of damage, and the damage could continuously accumulate under the increase in gravity loading produced by column or wall removal. This eventually could reduce the load-carrying capacity of structural members such that they may experience a dynamic failure under gravity load and, in turn, trigger progressive collapse of the whole structure. As indicated by the simulations, the time delay of the collapse depends largely on the predamage level during the column removal process and the level of sustained gravity load after column removal. In practice, if a building suffers severe structural damage, it is likely that the occupants will be evacuated from the building. Therefore, it may not be of particular interest to study a time delay that is beyond several days. Nevertheless, the present results show that, depending on the loading level, the delayed collapse could occur on the timescale of hours or a day (Fig. 8), which is within the operation time frame of first responders. This indicates that the time-dependent collapse is an important consideration for assessing structural vulnerability to progressive collapse.

Conclusions

A time-dependent cohesive element–based computational model for RC structures has been presented. The model captures two essential time-dependent behaviors of concrete: subcritical damage growth and viscoelastic deformation. The damage accumulation model is formulated based on continuum damage mechanics, and viscoelastic behavior is described using a nonaging compliance function. The model captures various nonlinear behaviors of materials, such as concrete material damage, reinforcement yield and rupture, and bond slip. The simulation of the NIST pushdown test indicated that the present model provides an efficient means of simulating the nonlinear response of RC structures under large deformation.

The model is successfully applied to investigate the time-dependent failure of a RC frame subassemblage under sustained loading. The simulation shows that the time-dependent behavior of concrete could lead to an intricate delayed failure of RC structures. The time delay in the failure response is largely governed by the predamage level and the level of sustained loading. The simulated load-lifetime curve can be well described by an inverse power law. At a considerable high loading level, the frame could fail on a timescale on the order of several hours.

Though the result of the present study may be perceived to be qualitative, it elucidates some key mechanisms that would lead to a delayed progressive collapse behavior of RC structures, which has been experimentally observed in recent studies. It is also shown that the time dependence of bond slip could have a considerable influence on delayed collapse behavior. The time-dependent failure mechanism represents a new consideration for assessing the vulnerability of buildings and structures against progressive collapse as part of the effort toward performance-based structural engineering.

Data Availability Statement

The computer code generated during the study is available from the corresponding author by request.

Acknowledgments

The authors deeply appreciate Dr. Bing Xue for stimulating discussion on the numerical implementation of the model in ABAQUS. They also acknowledge the University of Houston's Hewlett Packard Enterprise Data Science Institute for providing computational and IT resources for this work.

References

ACI (American Concrete Institute). 2003. *Bond and development of straight reinforcing bars in tension*. ACI 408R-03. Farmington Hills, MI: ACI.

ACI (American Concrete Institute). 2008. *Guide for modeling and calculating shrinkage and creep in hardened concrete*. ACI 209.2R-08. Farmington Hills, MI: ACI.

Alashker, Y., H. Li, and S. El-Tawil. 2011. "Approximations in progressive collapse modeling." *J. Struct. Eng.* 137 (9): 914–924. https://doi.org/10.1061/(ASCE)ST.1943-541X.0000452.

Alnaggar, M., G. Di Luzio, and G. Cusatis. 2017. "Modeling time-dependent behavior of concrete affected by alkali silica reaction in variable environmental conditions." *Materials* 10 (5): 471. https://doi.org/10.3390/ma10050471.

ASCE. 2010. *Minimum design loads for buildings and other structures*. ASCE/SEI 7-10. Reston, VA: ASCE.

Atkinson, B. K. 1984. "Subcritical crack growth in geological materials." *J. Geophys. Res.* 89 (B6): 4077–4114. https://doi.org/10.1029/JB089iB06p04077.

Bao, Y., S. K. Kunnath, S. El-Tawil, and H. S. Lew. 2008. "Macromodel-based simulation of progressive collapse: RC frame structures." *J. Struct. Eng.* 134 (7): 1079–1091. https://doi.org/10.1061/(ASCE)0733-9445(2008)134:7(1079).

Barenblatt, G. I. 1959. "The formation of equilibrium cracks during brittle fracture. General ideas and hypotheses. Axially-symmetric cracks." *J. Appl. Math. Mech.* 23 (3): 622–636. https://doi.org/10.1016/0021-8928(59)90157-1.

Bažant, Z. P., and L. Cedolin. 1991. *Stability of structures: Elastic, inelastic, fracture and damage theories*. New York: Oxford University Press.

Bažant, Z. P., and M. Jirásek. 2018. *Creep and hygrothermal effects in concrete structures*. Dordrecht, Netherlands: Springer.

Bažant, Z. P., and J.-L. Le. 2017. *Probabilistic mechanics of quasibrittle structures: Strength, lifetime, and size effect*. Cambridge, UK: Cambridge University Press.

Bažant, Z. P., J.-L. Le, and M. Z. Bažant. 2009. "Scaling of strength and lifetime distributions of quasibrittle structures based on atomistic fracture mechanics." *Proc. Natl. Acad. Sci.* 106 (28): 11484–11489. https://doi.org/10.1073/pnas.0904797106.

Bažant, Z. P., J.-L. Le, F. R. Greening, and D. B. Benson. 2008. "What did and did not cause collapse of WTC twin towers in New York." *J. Eng. Mech.* 134 (10): 892–906. https://doi.org/10.1061/(ASCE)0733-9399(2008)134:10(892).

Bažant, Z. P., and W. P. Murphy. 1995. "Creep and shrinkage prediction model for analysis and design of concrete structures: Model B_3." *Mater. Struct.* 28 (6): 357–365. https://doi.org/10.1007/BF02473152.

Bažant, Z. P., and J. Planas. 1998. *Fracture and size effect in concrete and other quasibrittle materials*. London: CRC Press.

Bažant, Z. P., and S. Prasannan. 1989. "Solidification theory for concrete creep. I: Formulation." *J. Eng. Mech.* 115 (8): 1691–1703. https://doi.org/10.1061/(ASCE)0733-9399(1989)115:8(1691).

Bažant, Z. P., and P. C. Prat. 1988. "Effect of temperature and humidity on fracture energy of concrete." *ACI Mater. J.* 85 (4): 262–271.

Bažant, Z. P., and M. Verdue. 2007. "Mechanics of progressive collapse: Learning from world trade center and building demolitions." *J. Eng. Mech.* 133 (3): 308–319. https://doi.org/10.1061/(ASCE)0733-9399(2007)133:3(308).

Bažant, Z. P., and Y. Xi. 1995. "Continuous retardation spectrum for solidification theory of concrete creep." *J. Eng. Mech.* 121 (2): 281–288. https://doi.org/10.1061/(ASCE)0733-9399(1995)121:2(281).

Bažant, Z. P., Q. Yu, and G.-H. Li. 2012. "Excessive long-time deflections of collapsed pre-stressed box girders. II: Numerical analysis and lessons learned." *J. Struct. Eng.* 138 (6): 687–696. https://doi.org/10.1061/(ASCE)ST.1943-541X.0000375.

Boumakisa, I., G. Di Luzio, M. Marcon, J. Vorel, and R. Wan-Wendner. 2018. "Discrete element framework for modeling tertiary creep of concrete in tension and compression." *Eng. Fract. Mech.* 200 (Sep): 263–282. https://doi.org/10.1016/j.engfracmech.2018.07.006.

BSI (British Standard Institute). 2006. *Actions on structures. 1–7: General actions—Accidental actions*. BS EN 1991-1-7. London: BSI.

Carpinteri, A., S. Valente, F. P. Zhou, G. Ferrara, and G. Melchiorri. 1997. "Tensile and flexural creep rupture tests on partially-damaged concrete specimens." *Mater. Struct.* 30 (5): 269–276. https://doi.org/10.1007/BF02486351.

Di Luzio, G. 2009. "Numerical model for time-dependent fracturing of concrete." *J. Eng. Mech.* 135 (7): 632–640. https://doi.org/10.1061/(ASCE)0733-9399(2009)135:7(632).

DoD (Department of Defense). 2009. *Design of buildings to resist progressive collapse*. UFC-4-023-03. Washington, DC: DoD.

Dugdale, D. S. 1960. "Yielding of steel sheets containing slits." *J. Mech. Phys. Solids* 8 (2): 100–104. https://doi.org/10.1016/0022-5096(60)90013-2.

Evans, A. G. 1972. "A method for evaluating the time-dependent failure characteristics of brittle materials and its application to polycrystalline alumina." *J. Mater. Sci.* 7 (10): 1146–1173. https://doi.org/10.1007/BF00550196.

Evans, A. G., and Y. Fu. 1984. "The mechanical behavior of alumina." In *Fracture in ceramic materials*, 56–88. Park Ridge, NJ: Noyes Publications.

Gardner, N. J., and M. J. Lockman. 2001. "Design provisions for drying shrinkage and creep of normal strength concrete." *ACI Mater. J.* 98 (2): 159–167. https://doi.org/10.14359/10199.

Grierson, D. E., L. Xu, and Y. Liu. 2005. "Progressive-failure analysis of buildings subjected to abnormal loading." *Comput.-Aided Civ. Infrastruct. Eng.* 20 (3): 155–171. https://doi.org/10.1111/j.1467-8667.2005.00384.x.

GSA (General Services Administration). 2003. *Progressive collapse analysis and design guidelines for new federal office buildings and major modernization projects*. Washington, DC: GSA.

Hedegaard, B. D., C. E. W. French, and C. K. Shield. 2017. "Time-dependent monitoring and modeling of I-35W St. Anthony Falls bridge. II: Finite element modeling." *J. Bridge Eng.* 22 (7): 04017026. https://doi.org/10.1061/(ASCE)BE.1943-5592.0001054.

Helmy, H., H. Salem, and S. Mourad. 2012. "Progressive collapse assessment of framed reinforced concrete structures according to UFC guidelines for alternative path method." *Eng. Struct.* 42 (Sep): 127–141. https://doi.org/10.1016/j.engstruct.2012.03.058.

Husak, A. D., and E. M. Krokosky. 1971. "Static fatigue of hydrated cement concrete." *ACI J. Proc.* 68 (4): 263–271. https://doi.org/10.14359/11327.

ICC (International Code Council). 2009. *International building code*. Washington, DC: ICC.

Kachanov, L. 1986. *Introduction to continuum damage mechanics: Mechanics of elastic stability, 10*. Dordrecht, Netherlands: Springer.

Kachanov, M. 1994. "On the concept of damage in creep and in the brittle-elastic range." *Int. J. Damage Mech.* 3 (4): 329–337. https://doi.org/10.1177/105678959400300402.

Kaewkulchai, G., and E. B. Williamson. 2004. "Beam element formulation and solution procedure for dynamic progressive collapse analysis." *Comp. Struct.* 82 (7–8): 639–651. https://doi.org/10.1016/j.compstruc.2003.12.001.

Khandelwal, K., and S. El-Tawil. 2008. "Pushdown resistance as a measure of robustness in progressive collapse analysis." *Eng. Struct.* 33 (9): 2653–2661. https://doi.org/10.1016/j.engstruct.2011.05.013.

Kunnath, S. K., Y. Bao, and S. El-Tawil. 2018. "Advances in computational simulation of gravity-induced disproportionate collapse of RC frame buildings." *J. Struct. Eng.* 144 (2): 03117003. https://doi.org/10.1061/(ASCE)ST.1943-541X.0001938.

Le, J.-L., and B. Xue. 2014. "Probabilistic analysis of reinforced concrete frame structures against progressive collapse." *Eng. Struct.* 76 (Oct): 313–323. https://doi.org/10.1016/j.engstruct.2014.07.016.

Lemaitre, J., and R. Desmorat. 2005. *Engineering damage mechanics: Ductile, creep, fatigue and brittle failures*. Berlin: Springer.

Lew, H. S., Y. Bao, F. Sadek, and J. A. Main. 2011. *An experimental and computational study of reinforced concrete assemblies under a column removal scenario*. NIST Technical Note 1720. https://doi.org/10.6028/NIST.TN.1720.

Lowes, L. N., and A. Altoontash. 2003. "Modeling reinforced concrete beam-column joints subjected to cyclic loading." *J. Struct. Eng.* 129 (12): 1686–1697. https://doi.org/10.1061/(ASCE)0733-9445(2003)129:12(1686).

Masoero, E., F. K. Wittel, H. J. Herrmann, and B. M. Chiaia. 2010. "Progressive collapse mechanisms of brittle and ductile framed structures." *J. Eng. Mech.* 136 (8): 987–995. https://doi.org/10.1061/(ASCE)EM.1943-7889.0000143.

Pesce, C. P., L. Casetta, and F. M. dos Santos. 2012. "Equation of motion governing the dynamics of vertically collapsing buildings." *J. Eng. Mech.* 138 (12): 1420–1431. https://doi.org/10.1061/(ASCE)EM.1943-7889.0000453.

Rabotnov, Y. N. 1969. *Creep problems in structural members*. Amsterdam, Netherlands: North-Holland.

Rüsch, H. 1960. "Research toward a general flexural theory for structural concrete." *J. Am. Concr. Inst.* 57 (1): 1–28.

Sadek, F., J. M. Main, H. S. Lew, and Y. Bao. 2011. "Testing and analysis of steel and concrete beam-column assemblies under a column removal scenario." *J. Struct. Eng.* 137 (9): 881–892. https://doi.org/10.1061/(ASCE)ST.1943-541X.0000422.

Sasani, M., and S. Sagiroglu. 2008. "Progressive collapse resistance of hotel San Diego." *J. Struct. Eng.* 134 (3): 478–488. https://doi.org/10.1061/(ASCE)0733-9445(2008)134:3(478).

Sezen, H., and J. P. Moehle. 2003. "Bond-slip behavior of reinforced concrete members." In *Proc., fib-Symp. (CEB-FIP): Concrete Structures in Seismic Regions*. Lausanne, Switzerland: International Federation for Structural Concrete.

Thouless, M. D., C. H. Hsueh, and A. G. Evans. 1983. "A damage model of creep crack growth in polycrystals." *Acta Metall.* 31 (10): 1675–1687. https://doi.org/10.1016/0001-6160(83)90166-9.

Xiao, Y., S. Kunnath, F. W. Li, Y. B. Zhao, H. S. Lew, and Y. Bao. 2015. "Collapse test of a 3-story half-scale RC frame building." *ACI Struct. J.* 112 (4): 429–438. https://doi.org/10.14359/51687746.

Xue, B., and J.-L. Le. 2016a. "Simplified energy-based analysis of collapse risk of reinforced concrete buildings." *Struct. Saf.* 63 (Nov): 47–58. https://doi.org/10.1016/j.strusafe.2016.07.003.

Xue, B., and J.-L. Le. 2016b. "Stochastic computational model for progressive collapse of reinforced concrete buildings." *J. Struct. Eng.* 142 (7): 04016031. https://doi.org/10.1061/(ASCE)ST.1943-541X.0001485.

Zhou, F. P. 1992. "Time-dependent crack growth and fracture in concrete." Ph.D. thesis, Dept. of Building Technology, Lund Institute of Technology.